Int J CARS (2016) 11:1515–1526
DOI 10.1007/s11548-015-1339-2

ORIGINAL ARTICLE

A novel method for texture-mapping conoscopic surfaces for minimally invasive image-guided kidney surgery

Rowena Ong[1] · Courtenay L. Glisson[2] · Jessica Burgner-Kahrs[4] · Amber Simpson[3] · Andrei Danilchenko[7] · Ray Lathrop[5] · S. Duke Herrell[6] · Robert J. Webster III[5] · Michael Miga[2] · Robert L. Galloway[2]

Received: 5 June 2015 / Accepted: 9 December 2015 / Published online: 13 January 2016

Abstract *Purpose* Organ-level registration is critical to image-guided therapy in soft tissue. This is especially important in organs such as the kidney which can freely move. We have developed a method for registration that combines three-dimensional locations from a holographic conoscope with an endoscopically obtained textured surface. By combining these data sources clear decisions as to the tissue from which the points arise can be made.

Methods By localizing the conoscope's laser dot in the endoscopic space, we register the textured surface to the cloud of conoscopic points. This allows the cloud of points to be filtered for only those arising from the kidney surface. Once a valid cloud is obtained we can use standard surface registration techniques to perform the image-space to physical-space registration. Since our methods use two distinct data sources we test for spatial accuracy and characterize temporal effects in phantoms, ex vivo porcine and human kidneys. In addition we use an industrial robot to provide controlled motion and positioning for characterizing temporal effects.

Results Our initial surface acquisitions are hand-held. This means that we take approximately 55 s to acquire a surface. At that rate we see no temporal effects due to acquisition synchronization or probe speed. Our surface registrations were able to find applied targets with submillimeter target registration errors.

Conclusion The results showed that the textured surfaces could be reconstructed with submillimetric mean registration errors. While this paper focuses on kidney applications, this method could be applied to any anatomical structures where a line of sight can be created via open or minimally invasive surgical techniques.

Keywords Image-guided surgery · Kidney surgery · Minimally invasive surgery · Conoscopy

✉ Robert L. Galloway
bob.galloway@vanderbilt.edu

Rowena Ong
rowena.e.ong@medtronic.com

Courtenay L. Glisson
Courtenay.l.Glisson@vanderbilt.edu

Jessica Burgner-Kahrs
burgner-kahrs@mzh.uni-hannover.de

Andrei Danilchenko
andreinash@gmail.com

Ray Lathrop
ray.a.lathrop@vanderbilt.edu

S. Duke Herrell
duke.herrell@vanderbilt.edu

Robert J. Webster III
Robert.webster@vanderbilt.edu

Michael Miga
Michael.Miga@vanderbilt.edu

[1] Medtronic Surgical Technologies, Louisville, CO 80027, USA

[2] Department of Biomedical Engineering, Vanderbilt University, Nashville, TN 37235, USA

[3] Memorial Sloan Cancer Center, New York City, NY, USA

[4] Hannover Center of Mechatronics, Leibniz Universität Hanover, Hanover, Germany

[5] Department of Mechanical Engineering, Vanderbilt University, Nashville, TN 37235, USA

[6] Department of Urologic Surgery, Vanderbilt Medical Center, Nashville, TN 37235, USA

[7] MAKO Surgical, Ft. Lauderdale, FL, USA

Introduction

The National Cancer Institute Surveillance Epidemiology and End Result (NCI-SEER) Statistics Review estimates that there were 63,390 new cases of renal cancer and 13,860 deaths in 2014. Unlike cancer rates in general, kidney cancer occurrences continue to climb. For localized cases, complete resection is the primary curative treatment [1]. Traditionally, radical nephrectomy, encompassing resection of one entire kidney, the surrounding fat and lymphatics, and the adrenal gland, was the recommended treatment for patients [2]. More recently, partial resection of the kidney (partial nephrectomy) has become the preferred form of treatment due to improved surgical techniques. This is demonstrated in Fig. 1 from Cooperberg et al. [3]. Discovery of earlier stage and thus smaller carcinomas, via continuously improving medical imaging devices and techniques, enables, if not mandates, partial nephrectomy techniques. A partial nephrectomy involves the removal of the diseased segment of renal tissue while leaving the largest possible amount of normal functioning kidney tissue [4]. With the ability to detect carcinomas early, the diseased tissue is more localized to the kidney with the absence of metastasis, thus increasing the number of candidates for a partial nephrectomy or ablation procedures. Recent studies have demonstrated that a partial nephrectomy, either open or laparoscopic, is an effective procedure for renal cell carcinoma and is especially applicable for tumors less than 4 cm [5–8]. In addition to providing equivalent oncologic outcomes, improved patient morbidity and mortality, as compared to complete kidney removal, have been noted. Nephron-sparing procedures are imperative when the contralateral kidney is functionally impaired or has been surgically removed [9,10].

The balance of sparing as many nephrons as possible while completely treating the diseased kidney tissue is crucial in kidney surgery for cancer as well as benign disease processes. The therapeutic challenge can be divided into three tasks: defining the margin of the diseased tissue, guiding the therapeutic process to this area and defining the effective therapeutic zone. However, there are several technical challenges associated with these procedures including adequate intraoperative identification of the margins of the diseased tissue, identification and control of the vascular supply, and avoidance of ischemic injury to the normal kidney tissue [11]. Currently, surgeons remove the diseased tissue using visualization, either directly or via a lens. However, this is problematic because the appearance of diseased and normal tissue may not be significantly different. This can prolong the procedure and decreases the likelihood of a clear margin without significant excess healthy tissue damage. Surgeons are often forced to resect a target that they can barely see unless they significantly disturb healthy tissue. The less the surgeons are required to disturb the kidney and its surrounding tissue during the procedure, the shorter the recovery time will be for the patient. Thus, there remains a need to improve intraoperative visualizations of the kidney in order to improve surgical outcome; for example, this includes a display of the present position of surgical instruments using the three-dimensional data of the preoperative tomograms. Employing image-guided surgery techniques, which are now a standard in neurosurgery and emerging in other abdominal surgeries, could provide these visualizations during the pro-

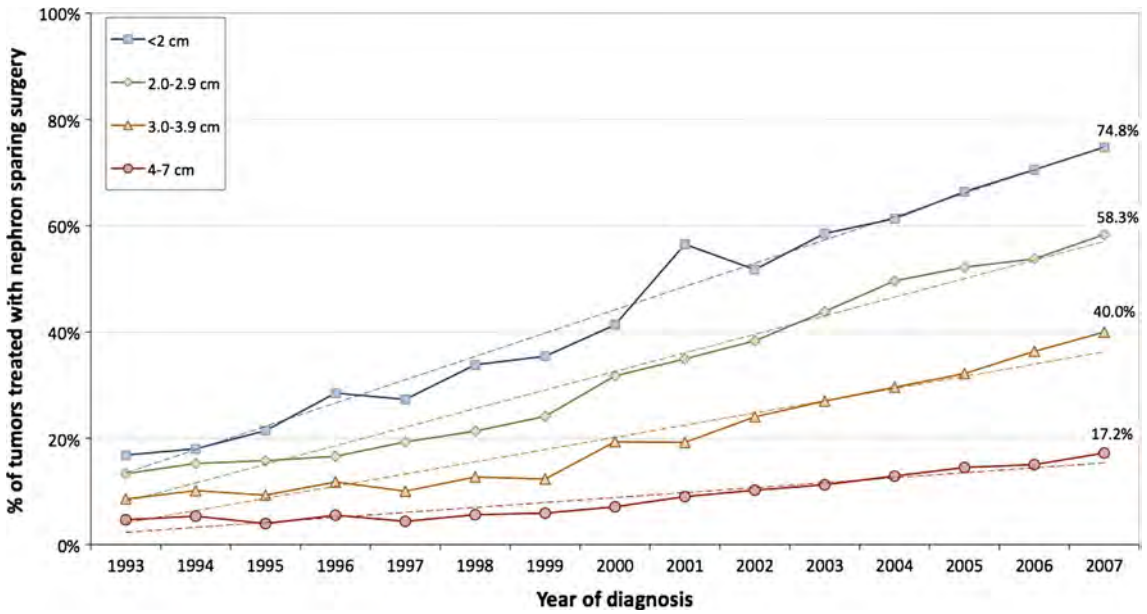

Fig. 1 Growth of kidney cancer resection via partial nephrectomies by year. From [3]

cedure. The definition of a successful partial nephrectomy is the resection or ablation of a renal lesion while sparing as many nephrons as possible. The largest source of surgical morbidity for either resection or ablation is vascular injury [12]. Therefore, both the success of the resection and the minimization of morbidity would be augmented by active display of surgical tool position relative to the location of the preoperatively determined surgical margin and the surrounding vasculature. As a result, more partial nephrectomies could be performed for masses currently treated with radical nephrectomy with vascular damage minimized and increased preserved renal function, resulting in improvement in patient outcomes.

The treatment of kidney tumors is also becoming less invasive, with the development of minimally invasive surgical techniques (MIS) [13] and even percutaneous procedures [14]. The success of any style of kidney tumor treatment process—surgery, radiofrequency ablation, cryoablation or others—can be defined as complete elimination of the lesion with minimum damage to healthy nephrons and vital structures. Therefore, the margins of the lesion must be assessed pre-operatively, the healthy structures of interest must be localized, and the desired treatment zone resected or ablated. If this information can be provided interactively during surgery, then margins can be closely resected while minimizing damage to healthy structures. However, any decision based on preoperative images requires both an image-space to physical-space registration and understanding of the factors that determine the quality of that registration.

We have demonstrated surface-based kidney registration in open procedures [15] and demonstrated that the quality of registration is dependent on both the amount and the location of the surface(s) used for the registration [16]. Involving highly figured (large changes in curvature) segments of the kidney promotes a better registration as does the use of a wide range of surface orientations such as the two poles of the kidney. This was also demonstrated by Puerto-Sueza and Mariottini [17]. Lastly, we have demonstrated [18] a point-based registration in human surgeries which builds on our initial surface-based registration. This secondary method is not optically based and thus allows us to rapidly re-register throughout a procedure in the face of smoke and even deformations due to resection. However, this secondary registration is dependent on having a high-quality initial surface registration.

A number of surface acquisition processes have been developed. These include a laser range scanner (LRS) [19], stereo pair [20], structured light [21] and time-of-flight camera [22] systems. An excellent review of most of these methods appears in [23]. The LRS and time-of-flight endoscopy have been successfully used in liver and brain registrations [24–27]. However they are obtained, the physical data used for the registration are not a mathematical surface but rather a cloud of points sampled from the physical surface of the organ.

In kidney surgery there is a relatively rigid organ [15], which is clamped in place at the start of the resection. In addition, the renal capsule is smooth and softly curved with a convex lateral side and a deeply grooved concave medial side forming the hilum. A robust registration methodology will require capturing this surface with significant curvature information to "lock in" the registration. We have significant experience using a LRS to capture surface information during surgery [19,24,25]. However, as the procedure progresses to minimally invasive approaches the LRS is too large to be used through a laparoscopic trocar.

To address this issue, we have been exploring conoscopic holography for intraoperative data collection in minimally invasive surgeries. The conoprobe is composed of a six-dimensional tracking system (Polaris optical tracking system Northern Digital, Ontario, Canada) rigidly mounted onto a conoscope. Conoscopic data acquisition consists of a laser transmitted from the conoscope aperture and reflected back to the detector. The conoscope provides a distance measurement which can then be translated into a 3D point via the transformation matrix determined during calibration. The conoscope is then moved to acquire another point in the physical-space cloud. The cost of this method is building the physical-space data cloud via repeated point acquisition. The advantage of this method is that the conoscope can be moved within the trocar to interrogate complex curved surfaces. While the initial surface registration initially takes 1 minute, it allows us to establish correspondence between points on the surface of the organ and homologous points on the scan. With those points subsequent re-registrations take less than a second [34]. With the kidney clamped during the initial registration it is not moved by respiration or cardiac oscillations. We consider the temporal cost of this initial registration to be reasonable since it gives us a high-quality registration which allows us to establish point correspondence for fast re-registrations as the surgery proceeds.

The conoprobe passes the reflected light through a polarizer and crystal, and the resulting phase changes and interference pattern can be used to calculate the distance to the object [28,29]. When optically tracked, the conoscopic laser can be swept across an organ surface to obtain a 3D point cloud [30]. An accuracy study of the geometric surface obtained by an optically tracked conoscope can be found in [31], and registration accuracy studies have also been performed [32].

We have demonstrated that a surface can be obtained with the conoscope (surface scanning); however, one important question remains. How do we know that the surface obtained is the surface we desire for organ-level registration? Is the geometric information from conoscopically obtained points sufficient to identify the organ in question or is error introduced from misidentification of surrounding tissue? In the

case of the kidney, can the conoscope points be ascribed entirely to the kidney or are some fraction of them from the perinephric fat? As a step toward an answer to this this question we have developed a novel method of texture-mapping the conoscope-obtained surface using a laparoscopic camera. This process is a form of feature tracking although we do not use the acquired feature for registration. We will characterize both techniques independently and then combine them for a surface registration.

Methods

Our method combines two aspects. We have three-dimensional spatial points from the conographic holography system (the conoprobe) and we have two-dimensional texture points from the tracked endoscope. Those disparate data sets can be used to address the weaknesses of the other if they can be integrated spatially and temporally.

The stationary spatial performance of the conoprobe has been characterized in two previous papers [30,32]. There are two challenges with such points. First, because the organ lacks fiducial points we cannot count on correspondence between physical and image points for registration. Second, the acquired points arise from any surface reflection which may or may not be the desired organ surface. Our solution is to integrate an endoscopic image to allow texture mapping of the laser points. Once that texture is complete we can screen the conoscopic points for only those arising from the target of interest. This combination requires that we characterize the conoscopic and endoscopic systems separately and then measure the performance of the combined system. This characterization will include spatial and temporal sensitivities.

Conoscopic hardware

A commercially available conoscopic holography sensor (conoprobe) (Probe Head Mk3, OPTIMET, North Andover, MA) was used. To optically track its 3D location and orientation, a rigid body with retro-reflective marker spheres (Northern Digital, Ontario, Canada) was attached to the body of the conoscope (Fig. 2). A sterilizable, airtight attachment was constructed to facilitate its use through a laparoscopic trocar port. The conoscope data rate can be set as high as 1000 Hz, but for these experiments, we used a sampling frequency of 400 Hz (2.5 ms period). This rate was selected because the data transfer rate has a 1ms frame latency, and by allowing 2.5 latency units between samples we are assured of a unique data acquisition per frame.

The rigid body coupled with the Polaris optical tracking system (Northern Digital, Ontario, Canada) provides us with six degree of freedom tracking. By calibrating the location and direction of the laser beam with respect to the rigid body

Fig. 2 Conoscope with Polaris rigid body attached

we can determine the location of the reflection point of the conoprobe's laser by combining the distance measurement from the conoprobe with the pose information from the optical tracking system. To obtain the transformation from the Polaris rigid body center to the conoprobe origin, a calibration was performed using a pivot technique. The details and error analysis of this calibration can be found in [31].

Laparoscopic video collection

In addition to the tracked conoprobe, a rigid laparoscope is targeted at the organ to capture the visible field of view in physical space. We performed experiments with both Karl Storz Telecam NTSC and Tricam SL NTSC and Karl Storz Xenon Light Source 615 and 175. As the conoprobe captures the 3D surface locations, the laparoscopic video frames are grabbed. To capture the frames we used an Elgato Video Capture frame grabber that ports S-video to USB. A program was written to capture the video stream using the API of Microsoft's DirectShow on a Windows 7 laptop. The laparoscope has a frame rate of 30 Hz with one frame latency. A Polaris tracker is rigidly attached to the scope and a calibration block is scanned before every application. The 16 targets on the block are known to a NIST-traceable 0.25 mm and a 3-D to 2-D transformation is calculated [31–33].

Texture mapping algorithm

In this method, an optically tracked conoprobe is swept across a surface to obtain a 3D point cloud. This point cloud is then texture mapped using the video obtained from the laparoscopic camera. To texture map the point cloud, we use the fact that each 3D point has a corresponding video frame in which the red laser dot is seen. From the segmented red dot, the texture coordinates of the point can be determined, and a color

can be assigned from either a reference image or a previous frame. The color texture is interpolated into the remaining image via thin-plate splines. The segmentation looks for a collection of connected red pixels and fits their distribution to Gaussian shape. The centroid of that shape becomes the selected point. In our implementation, we assume the laparoscopic camera is fixed while the conoprobe is moved during the data acquisition, and we assign the texture from a reference image taken before the conoprobe acquisition. There is no assumption of tissue-to-scope distance. However, because we can track the laparoscopic camera it is simple to place both objects in a single reference frame.

Synchronization

There are four time-dependent processes in the use of the conoprobe to obtain a surface for image-to-surface registration: (1) data acquisition rate and latency of the conoprobe, (2) data acquisition rate and latency of the Polaris, (3) the frame rate and latency of the video camera and (4) the sweeping motion of the conoprobe over the target organ. The temporal relationship of all four must be investigated to ensure proper geometric and texture rendering of the organ data. The first three, conoprobe, Polaris and laparoscope, have fixed rates and latencies, and their data streams have to be synchronized to ensure an accurate 3D point location (Polaris and conoprobe) and accurate color texture (laparoscope). In contrast, the fourth time-related event, the motion of the conoprobe can be varied. We performed experiments to test the interaction of conoprobe motion with the first three factors.

A custom, multithreaded C++ program was implemented to obtain the conoscopic, Polaris and video. The conoprobe and Polaris data were time-stamped using the standard Windows libraries. For the video stream, a time-stamp was obtained at the start of the stream, and the relative timing of the frames was saved as a part of the video format. Each data stream was post-processed to match the frames in each data stream by timestamp. The frequency of the data streams was as follows: the Polaris at 60 Hz, the conoprobe at 400 Hz (for this application) and the video at 30 Hz.

Because the synchronization of the conoprobe, Polaris and video data streams is a deciding factor for the achievable texture-mapping accuracy, we performed a series of tests to quantify the synchronization accuracy. There are several sources of possible synchronization error: (1) determination of start time of video stream, (2) relative timing of each frame of the video stream, (3) Polaris temporal resolution, (4) conoprobe timing. Both differences in rate and latency can be accounted for in these experiments. These studies are important to determine whether there is differential latency (which we would see as a temporal offset) or a lack of synchronization (which we would see as data temporal drift), and if so, whether we can correct it. The final synchronization accuracy will place a limit on the accuracy of the texture map as well as the conoprobe scanning speed. In addition, characterizing the synchronization error will also help us determine what frame rates we need in the future if a certain scan speed or accuracy is desired.

In a first test we used a commonly employed external blocking event to verify the synchronization of the conoprobe, Polaris and video data streams. An object was dropped in front of an aligned Polaris target, conoprobe laser and laparoscopic camera such that it would block all data streams simultaneously. The times of the blocking event were found in each data stream and compared to find both the error and any offset. As the conoprobe had the highest temporal resolution, it was used as the reference and the Polaris and video streams were synchronized to it.

In a second experiment, we sought to verify the relative timing accuracy of the video stream, in particular to determine whether there was a drift or bias over time. Because only the starting time of the video stream is recorded, it was important to verify the relative accuracy of the timestamps in the saved video format. To do this, we aimed the laparoscopic camera at an external millisecond clock displayed on the screen of a separate laptop. For three trials and at seven different sampling times ranging from 5 to 180 s into the video stream, the difference between the external timer and the internal video timing was determined for a total of 21 samples.

Accuracy studies

As the geometric accuracy of the conoscopic surface has been characterized previously [33], in this paper we focus on characterizing the accuracy of the texture map. This includes determining the effects of the laparoscopic sweep speed on the texture map accuracy.

Because the physical-space cloud is composed of points collected as the conoprobe is swept across a surface, the accuracy of the texture mapped surface may be dependent on the density of scan lines or the scan speed. To determine the effect of these factors on the texture accuracy, we used a robot (Mitsubishi RV-3S) to move the conoprobe at different speeds and different scan line spacings over a colored checkerboard image of known dimensions (see Fig. 3). Detailed information on robot kinematics and setup can be found in [34].

To verify the accuracy of a textured surface, the error between the known geometry of the checkerboard was compared to that obtained from the textured surface. Specifically, the error was defined as the distance between the square corners localized from the texture and their known locations. The calibration image used was a 5×3 checkerboard colored with red, green and blue squares printed on flat, white paper. Each square had a width of 13.9 mm.

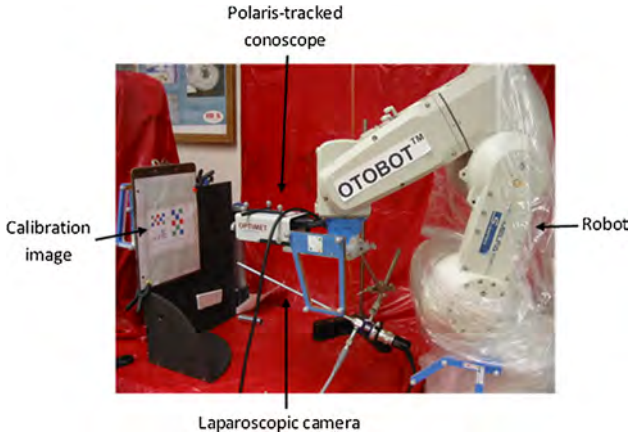

Fig. 3 Setup for the image calibration study. The robot aimed the tracked conoprobe across the calibration image, and multiple trials were taken using different scan line densities. The video obtained from the laparoscopic camera was used to texture map the conoscopic surface

To determine the effect of scan line density on the accuracy of the textured surface, we used the robot to obtain five datasets at 10-, 5- and 2-mm scan line spacing, for a total of 15 data acquisitions. The Polaris, conoprobe and laparoscopic video streams were synchronized, and the conoscopic surface was constructed and textured using the image processing methods described above. The checkerboard corners were localized from the textured surface manually, and the distance from the known locations was calculated.

In addition to scan line density, the effect of scan speed on texture accuracy was also investigated. The robot was used to aim the conoprobe across the checkerboard phantom at 20 and 40 mm/s at a line spacing of 10 mm. The accuracy of the conoscopic scans was calculated as described above.

Ex vivo porcine kidneys

Because the conoscopic laser interacts with tissue differently than with other materials, it is important to validate our conoscopic texturing method using a more realistic material and geometry. To this end, ex vivo porcine kidneys (frozen at about −10 °C immediately after resection and thawed before use) were scanned with the conoprobe and texture mapped using the presented method. Flat, circular green surface fiducials (diameter 7.2 mm) were marked with an "x" at their centers and used to calculate the texture accuracy. Two methods of validation were used in these studies: (1) comparison of the texture-localized fiducials to a gold standard localized using a probe and (2) comparison to an LRS texture.

Validation using probe-localized points

In these studies, four ex vivo porcine kidneys had surface fiducials applied (see Fig. 4). Depending on kidney size and surface curvature 5–11 surface fiducials were applied for validation. The fiducial centers were localized using either a Polaris probe or conoprobe as a gold standard, and the error between the texture-localized and gold standard positions was calculated. Because we had placed fiducials and thus had known correspondence, we could calculate a fiducial registration error (FRE), the mean RMS distance between the fiducial's actual image location and the location estimated by transforming the physical-space locations of the points into image space. Such a measure allows estimation of the device or processes' precision. True accuracy is determined by calculating the target registration error (TRE) of a point-based registration between the texture-localized and gold standard probe-localized fiducials. To do this, one fiducial was designated the target, while the remaining were used in the point-based registration. We accepted the fiducial to Polaris registration as the gold standard and used an iterative process to test for sensitivities to fiducial location. That iter-

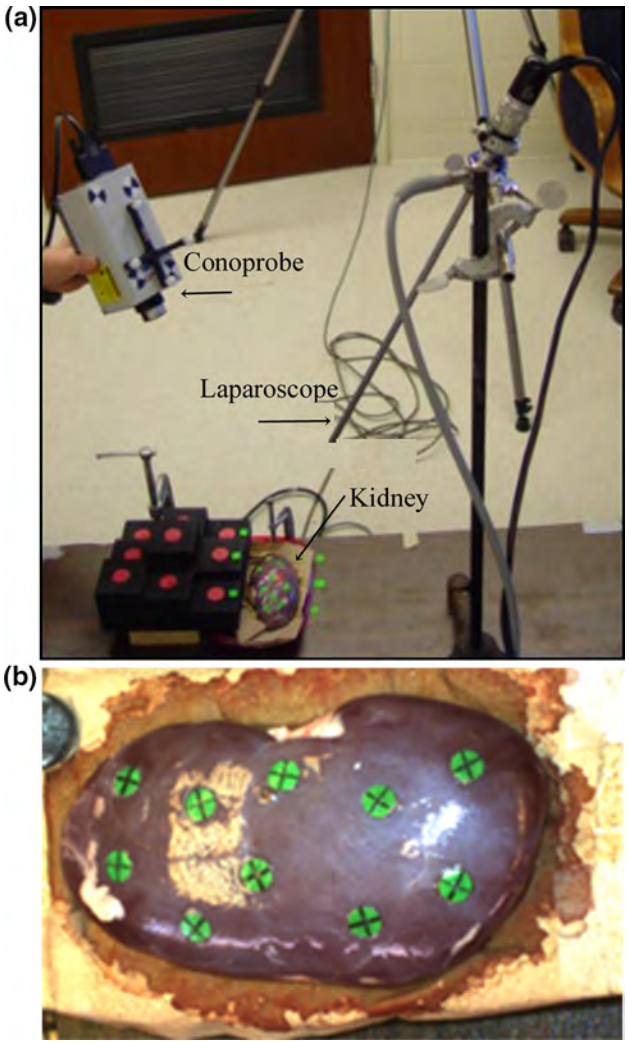

Fig. 4 Setup for ex vivo porcine kidney scans and close-up of porcine kidney covered with *circular green* surface fiducials

ative procedure repeated the localization each time changing the fiducial chosen as the target and the leave-one-out TRE was calculated at each fiducial. The leave-one-out TRE was then averaged over all the trials.

Comparison against a gold standard

To compare the conoscopic point cloud to that obtained from a gold standard LRS (Pathfinder Therapeutics, Inc, Nashville, TN), a porcine kidney was covered with 10 fiducials and scanned with a conoprobe five times, and the reconstructed textured surfaces were compared to an LRS scan. This comparison allowed the use of both a point-based registration since the fiducials provided correspondence and surface-based registration by comparing the point clouds obtained by use of the LRS and by the conoscope. The fiducial centers were localized from both the conoscopic texture and the LRS texture, and a point-based registration was used to align the two coordinate spaces. To measure the difference between the two surfaces, the FRE and leave-one-out TRE as described in the section above were calculated.

Ex vivo human kidneys

The accuracy of the conoscopic texture mapping was tested using an ex vivo kidney from a partially fixed human cadaver. To facilitate validation, six fiducials consisting of surgical tape marked with an "x" were attached to the kidney surface, and six conoscopic scans were obtained. The centers of the marks were localized using a Polaris probe, and the error between texture-localized and Polaris-localized points was calculated. The leave-one-out TRE and FRE were calculated as described in the previous section.

Scanning and post-processing times

The conoprobe scanning and post-processing times were recorded for the 10 ex vivo and four human cadaver trials. These post-processing scripts were run on with an Intel Core i7 processor, 4 GB of RAM and Windows 7 64-bit operating system installed.

Results

Synchronization studies

Synchronization studies with external blocking event

The synchronization studies indicated a delay between the Polaris and conoprobe data streams (mean 29.2 ms) and the laparoscope and the conoprobe (mean 0.55 frames). The positive sign of the errors indicates the synchronization event happened earlier in the conoprobe data stream than in the Polaris stream, and therefore, it appears that the Polaris stream is lagging behind the conoprobe. As the frame rate of the Polaris was 60 Hz, the mean delay was approximately 1.8 Polaris frames.

The video frames also lagged the conoprobe data, but by only an average of half a frame. Because of the relatively slow video frame rate (30 fps), and the difficulty in isolating the exact time of the synchronization event in the video frames, the delay of half a frame may be within the error of the measurements. What must also be considered is that this is a handheld surgical instrument, while it is possible to make the synchronizations significant by very rapidly moving the scope or the conoprobe, and in surgical reality this will not happen.

Accuracy of the relative timing of the video stream

There was no significant error in the relative timing of the video, as the mean difference between the external and internal timing was less than a millisecond (-0.4 ms $\pm$ 5.4 ms) over all the samples. There was also no bias or increase in error as the video progressed, as tested up to 180 s. The standard deviation was about 5 ms, which is within the error of the Windows C++ library used to obtain the times [37].

Accuracy studies

Calibration image

The effects of scan line density on texture map accuracy are shown in Fig. 5 for line spacings of 10, 5 and 2 mm. The mean errors in all cases were submillimetric (below 0.7 mm), and the maximum error did not exceed 2 mm. While the mean errors are slightly lower for denser line spacings, t test showed that these differences were not significant at the 0.05 confidence level. Some representative textured surfaces are shown in Fig. 6a. The quality of the texture maps generated from the denser scan lines appears to be slightly better than those generated from the more sparse lines.

To assess the effects of the scan speed on texture accuracy, the error of the textured surfaces was calculated from data taken at 20 mm/s and 40 mm/s. Figure 7 compares the mean error over all trials for data taken at a scan line spacing of 10 mm. The surfaces constructed from 20 mm/s data have a lower mean error than those from 40 mm/s. An ANOVA test showed that this difference is significant at the 0.05 confidence level, despite the small number of trials taken at 20 mm/s.

Ex vivo porcine kidney

Validation using probe-localized points

The textured surfaces constructed from ex vivo porcine kidneys were found to have submillimetric accuracy over

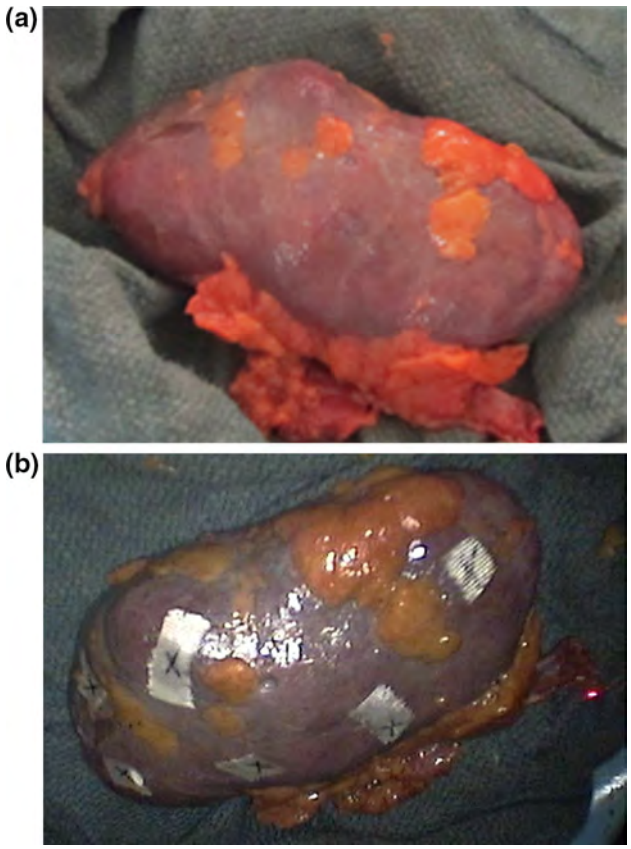

Fig. 5 Ex vivo kidneys from a partially fixed human cadaver to be scanned by the conoprobe (*left*); the same kidney covered with fiducial surface markers (*right*). The *peach-colored* areas represent the perirenal fat that had not been completely removed from the kidney

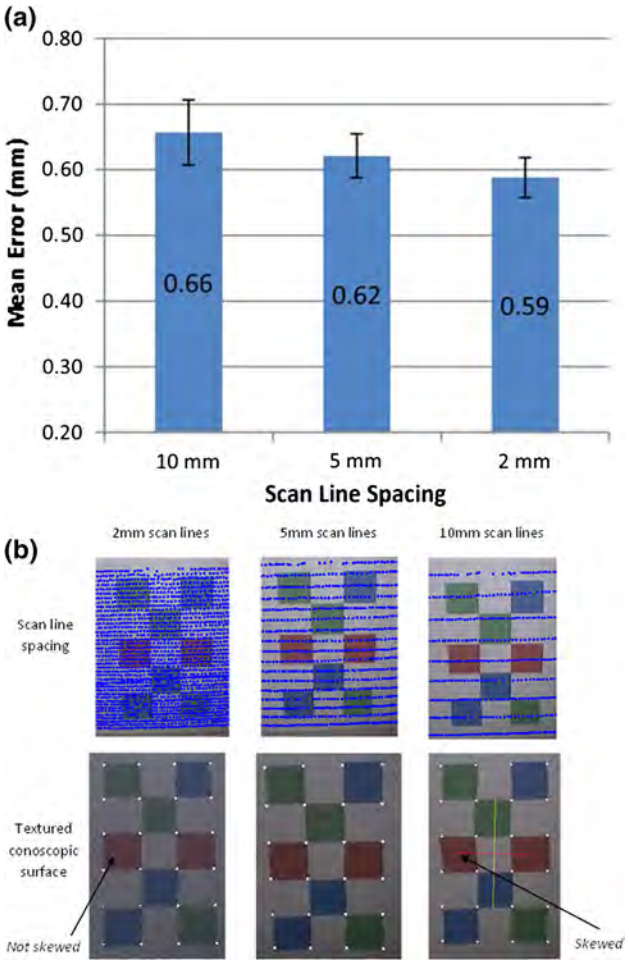

Fig. 6 **a** *Bar graph* showing the effect of scan line density on texture map accuracy, assessed using a checkerboard phantom. The *bars* show the mean error between texture-localized and known checkerboard corners, for five trials taken at scan line spacings of 10, 5 and 2 mm each. The speed of the robot data acquisition was 40 mm/s for all trials. The difference between the groups is not significant at the 0.05 confidence level, **b** representative textured surfaces constructed from data taken at 2, 5 and 10 mm scan line spacings. *Top row plots* showing the conoscopic line spacings that were used to construct each corresponding textured surface on the *lower row*. The *blue dots* represent the 3D points obtained by the conoscope. *Bottom row* textured conoscopic surfaces displayed with *white dots* representing actual locations of *square corners*. The letter *A* denotes an unskewed square, while the letter *B* denotes a skewed square constructed from the 10-mm line spacing

the 10 trials performed (see Fig. 8). The mean leave-one-out TRE and FRE over all trials was calculated to be 1.0 and 0.8 mm, respectively. The qualitative results can be seen in Fig. 9.

Comparison to LRS

While the previous studies validated the conoscopic texture using probe-localized points, a comparison with an LRS texture showed a submillimetric mean TRE and FRE over five trials (Fig. 10). While a total of 10 fiducials were used, small portions of some surfaces were not able to be constructed as the measurement volume of the optical tracking system was exceeded for some data. Therefore, in some cases, the fiducials in the small unconstructed areas were not able to be used. One representative result in Fig. 11 shows the LRS surface overlaid on the conoscopic surface. The small amount of error is apparent as shown by the white dots representing the conoscopic fiducial centers align quite well with the LRS surface.

Ex vivo human cadaver kidney

To verify the accuracy of the conoscopic texturing method on a human kidney, a point-based registration was performed between the fiducial stickers localized in the textured surface and those localized using a Polaris probe. The results are shown below in Table 1 and Fig. 12. The mean leave-one-out TRE over four trials was found to be 0.9 mm, with a maximum less than 1.5 mm.

Scanning and post-processing times

The mean scan time for 10 porcine and four human cadaver cases was found to be 56 ± 9 s, while the mean post-processing time was 35 ± 9 s. The total scan and post-

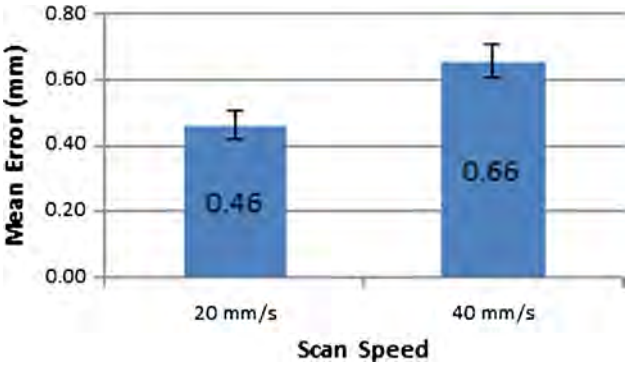

Fig. 7 *Bar chart* showing the effect of scan speed on texture accuracy, assessed using a checkerboard phantom and scan line spacing of 10 mm. The number of trials taken at 20 and 40 mm/s was 2 and 5, respectively. The increase in the error between 20 and 40 mm/s is significant at the 0.05 confidence level

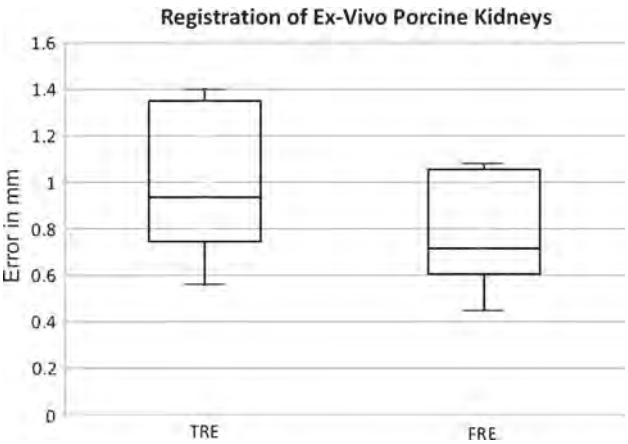

Fig. 8 Accuracy of the conoscopic textured surfaces from ex vivo porcine kidneys. The TRE and FRE of the point-based registrations between the gold standard probe-localized fiducials and the texture-localized fiducials are shown

processing time per case was found to be approximately 90 s. This is shown in Table 2. The post-processing steps have not yet been optimized for surgical workflow and will decrease dramatically when we can do so.

Discussion

Significance

In any image-guided surgical process two of the fundamental steps are establishing an image-space to physical-space registration and dealing with intraprocedural motion. By creating a methodology in which allows both a reasonable speed, initial, directable surface acquisition and one which allows intraoperative point-based rapid re-registration, we can address both concerns. By obtaining a textured three-dimensional surface, we have developed a technique applicable to image-guided minimally invasive kidney surgery.

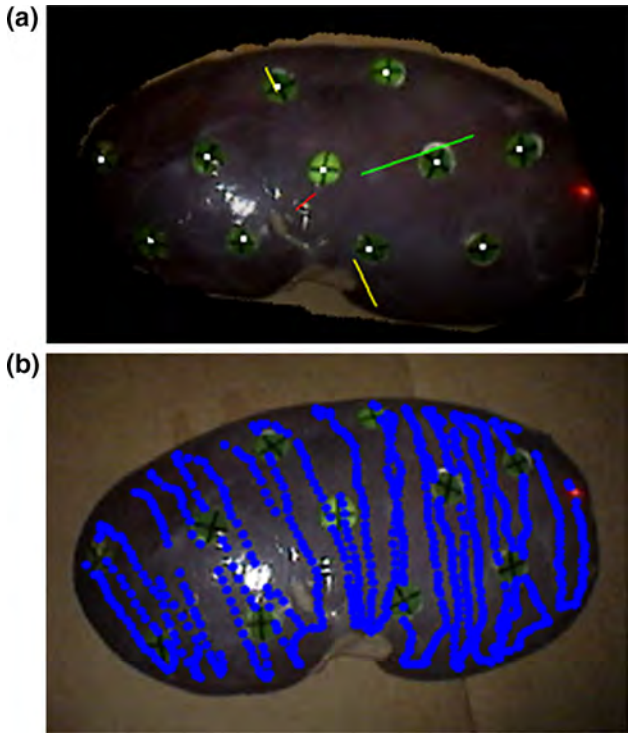

Fig. 9 *Left* textured conoscopic surface of ex vivo pig kidney covered in fiducials with *white dots* representing the true fiducial locations. *Right* the conoscopic points (*blue dots*) that were used to construct the surface

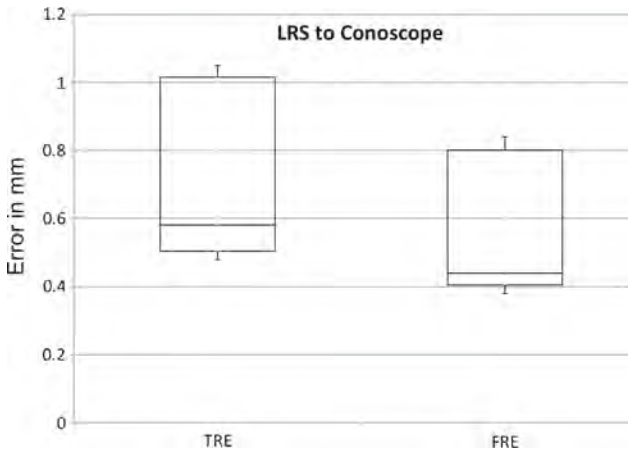

Fig. 10 Comparison between LRS and conoscopic surface textures for five different trials, with number of fiducials per trial ranging between 8 and 10. The leave-one-out TRE and FRE calculated between fiducials localized in the LRS and conoscopic textures are shown

We have extensive experience with organ-level surface-based image-space to physical-space registrations. With that experience comes caution in constructing the physical-space point clouds. An ICP-based registration will reduce the distances between the surfaces, but such mathematics can be confounded by rotationally symmetric surfaces. In addition we had concerns about moving to minimally invasive

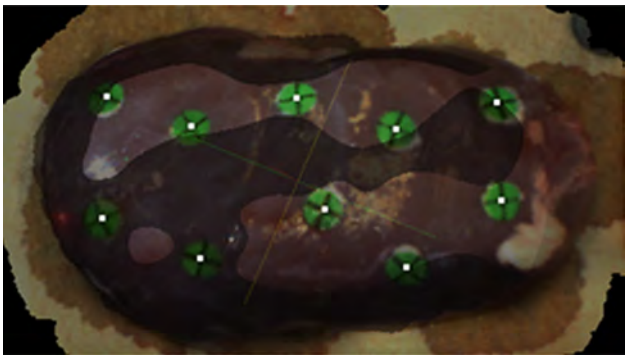

Fig. 11 LRS surface overlaid on conoscopic surface. *White dots* represent conoscopic fiducial centers

Table 1 Accuracy of the conoscopic textured surfaces taken from an ex vivo kidney from a human cadaver, for four different trials

TRE (leave-one-out) (mm)		FRE (mm)
Mean	Max	Mean
0.9	1.4	0.6

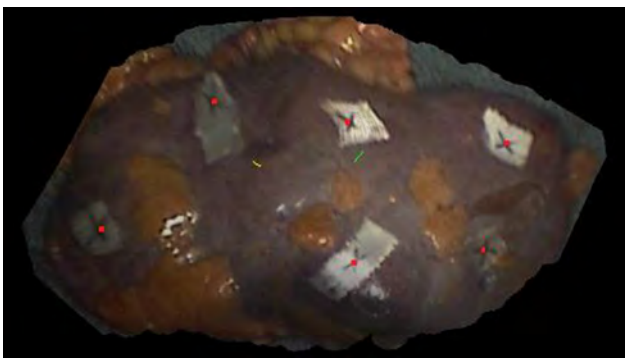

Fig. 12 Textured conoscopic surface of the ex vivo human cadaver kidney. The *white stickers* marked with an "x" are the fiducials, and the *red dots* represent the gold standard Polaris-localized positions

Table 2 Scanning and post-processing times for 10 porcine and four human cadaver cases

	Scan time (s)	Running time (s)		Total time (s)
		MATLAB	Python	
Mean	55.93	32.04	3.23	91.20
SD	8.69	8.18	1.92	16.42

scenarios because it is difficult to insure that the physical-space point cloud arises solely from the surface of the organ and not from surrounding tissue. By using the conoprobe–laparoscope combination we allow the direction of the point acquisition to include areas of high angular change such as the edges of the kidney or the hilum. Secondly we construct a texture on the surface of the point cloud to allow identification of "off target" points.

Calibration

It is easy to presume that all of the data channels are simultaneous but such a presumption can lead to unanticipated errors [35]. While latency and temporal misalignment have been explored in the augmented reality environment [36] they are occasionally overlooked as a source of data acquisition errors. Characterizing the synchronization error is important for several reasons. First, it is important to detect whether there is any offset or drift in the data streams so we can correct for it. Once any offset or drift is corrected, the final synchronization accuracy will place a limit on the accuracy of the texture map as well as the conoprobe scanning speed. For instance, larger errors in the synchronization can be offset by moving the conoprobe across the targeted object at a slower speed. Our results show that the synchronization was good enough for a hand-held surgical instrument. If we desire to move the system more quickly we are beginning to use more sophisticated techniques for the determination of synchronization issues to address faster scan speeds.

Scanning effects on accuracy

In the robot calibration studies described in this paper, we investigated the effects of scan speed and scan line density on textured surface accuracy. In the image calibration study, we found submillimetric mean errors for all scan line densities and scan speeds tested. The effect of scan line density for 2-, 5- and 10-mm line spacings was less pronounced than effects of scan speed. While we found slightly lower errors for denser line spacings, the difference was not found to be significant. The difference in error between the two scan speeds tested (20 and 40 mm/s) was more pronounced. In essence, this study implied that higher texture accuracy can be achieved by either increasing scan line density or decreasing scan speed, but decreasing scan speed may have a greater effect. In addition, the expected texture errors for 20 and 40 mm/s scans (0.33 and 0.66 mm, respectively) were on par with the observed mean errors (0.46 and 0.66 mm, respectively) assuming 1 frame of Polaris error. We recommend lower scan speeds (closer to 20 mm/s) for future systems. These studies are important because if it is desired to expand the use of the conoscopic acquisition to gather "patches" of surface and thus improve overall speed while retaining the ability to move the acquisition to convex and concave surfaces, we need to know the effects of acquisition speed.

Texture accuracy

In addition to the geometry, the texture accuracy was evaluated on a more realistic material, namely ex vivo pig kidneys. The error was calculated using three different gold standards

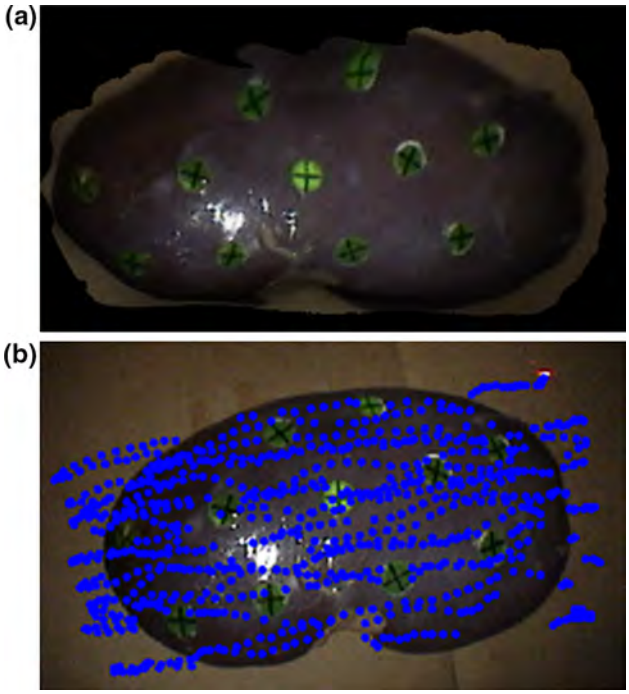

Fig. 13 Sources of surface error. In the *top image* the uppermost fiducial is elongated on reconstruction due to the surface interpolation. The *lower image* displays the conoscopic scan lines, which overshoot the kidney

to localize the fiducials: Polaris probe, conoprobe and LRS. While none of the gold standards are perfect, the mean leave-one-out TRE is consistently low and less than 1 mm. The submillimetric FRE indicates that the texture is not being distorted compared to the gold standards.

Another factor that we have observed affecting the textured surface accuracy was the proximity of the fiducial targets to the scan boundaries. The accuracy may degrade at edges if the points from which to interpolate are scarce and the curvature is high. Depending on the interpolation settings, the features at the edge may "bleed" outward. This can be seen in Fig. 13.

In the lower image in Fig. 13, the role of the texture is clearly seen. The overscan of the conoprobe would include points outside of the surface of the organ. This is reinforced by the image in Fig. 4 which shows the perinephric fat left on a "clean organ." In order to have confidence in the conoscopically derived surface, additional information in the form of texture mapping must be applied.

System performance

While our system is currently not set up to automatically process all the data after acquisition, this is a step that should not be difficult to achieve. Currently, a manual scan of a kidney takes an average of 55 s. The post-processing step running times take about 30 s and could be decreased if the algorithms were optimized for computational efficiency. Using a laparoscopic camera with higher frame rate and/or an optical tracking system with higher data acquisition rates would allow the conoprobe scan speeds to increase, enabling a decrease in the acquisition time or increase in scan line density.

Conclusion

In this paper, we have presented a novel method for texture mapping a 3D surface obtained by an optically tracked conoscopic holography sensor. Calibration and accuracy studies were performed using phantoms and ex vivo porcine kidneys covered with surface fiducials. The results showed that the textured surfaces could be reconstructed with submillimetric mean registration errors. These promising results indicate that it may be feasible to use the conoscopic textured surfaces to track intraoperative kidney motion for use in minimally invasive image guidance. Next steps include studies conducted in an in vivo porcine model; these have been performed and will be published in future publications.

Acknowledgments This work is funded in part by the National Institutes of Health: Grant R01 CA162477 from the National Cancer Institute, R01 NS049251 of the National Institute for Neurological Disorders and Stroke, and R44 DK081240 National Institute of Diabetes and Digestive and Kidney Diseases.

Compliance with ethical standards

Conflict of interest Rowena Ong, Courtenay Glisson, Jessica Burgner-Kahrs, Amber Simpson, Andrei Danilchenko, Ray Lathrop, Duke Herrell, Robert Webster III, Michael Miga, and Robert L. Galloway declare that they have no conflict of interest.

Human and animal participants The work used ex vivo kidneys obtained post-euthanasia from animals killed under IACUC-approved protocols. No human data were used.

References

1. Drucker BJ (2005) Renal cell carcinoma: current status and future prospects. Cancer Treat Rev 3:536–545. doi:10.1016/j.ctrv.2005.07.009
2. Patel SG, Penson DF, Clark PE, Cookson MS, Chang SS, Herrell SD, Smith JA, Borocase DA (2012) National trends in the use of partial nephrectomy: a rising tide that has not lifted all boats. J Urol 287(3):816–821. doi:10.1016/j.juro.2011.10.173
3. Cooperberg MR, Mallin K, Kane CJ, Carroll PR (2011) Treatment trends for stage 1 renal cell carcinoma. J Urol 186:394–399. doi:10.1016/j.juro.2011.03.130
4. Novick AC (2004) Laparoscopic and partial nephrectomy. Clin Cancer Res 10:6322S. doi:10.1158/1078-0432.CCR-050003
5. Orvieto M, Chien GW, Tolhurst SR, Rapp DE, Steinberg GD, Mikhail AA, Brendler CB, Shalhav AL (2005) Simplifying laparoscopic partial nephrectomy: technical considerations for repro-

ducible outcomes. Adult Urol 66:976–980. doi:10.1016/j.urology.2005.05.013
6. Fergany AF, Hafez KC, Novick AC (2000) Long-term results of nephron sparing surgery for localized renal cell carcinoma: 10-year followup. J Urol 163:442–445. doi:10.1016/S0022-5347(05)67896-2
7. Godley PA, Ataga KI (2000) Renal cell carcinoma. Curr Opin Oncol 12:260–264
8. Vogelzang NJ, Stadler WM (1998) Kidney cancer. Lancet 352:1691–1696. doi:10.1016/S0140-6736(98)01041-1
9. Nosnik IP, Mouraviev V, Nelson R, Polascik TJ (2006) Multiple nephron-sparing procedures in solitary kidney with recurrent, metachronous, nonfamilial renal cell carcinoma. Urology 68(6):1343. doi:10.1016/j.urology.2006.09.004
10. Lau WK, Blute ML, Weaver AL, Torres VE, Zincke H (2000) Matched comparison of radical nephrectomy vs nephron-sparing surgery in patients with unilateral renal cell carcinoma and a normal contralateral kidney. Mayo Clin Proc 75:1236–1242
11. Becker F, Van Poppel H, Hakenberg OW, Stief C, Gill I, Guazzoni G, Montorsi F, Russo P, Stöckle M (2009) Assessing the impact of ischaemia time during partial nephrectomy. Eur Urol 56(4):625–634. doi:10.1016/j.eururo.2009.07.016
12. Pomara G, Campo G, Francesca F (2009) Intraoperative and postoperative complications of nephron sparing surgery: prevention and possible treatments. Arch Ital Urol Androl 81(2):80–85
13. Kercher KW, Heniford PT, Matthews BD, Smith TI, Lincourt AE, Hayes DH, Eskind LB, Irby PB, Teigland CM (2003) Laparoscopic versus open nephrectomy in 210 consecutive patients: outcomes, cost, and changes in practice patterns. surg endosc 17(12):1889–1895
14. Negrete-Pulido O, Molina-Torres M, Castaño-Tostado E, Loske AM, Gutiérrez-Aceves J (2010) Percutaneous renal access: the learning curve of a simplified approach. J Endourol 24(3):457–460. doi:10.1089/end.2009.0210
15. Ong R, Glisson C, Altamar H, Viprakasit D, Clark P, Herrell SD, Galloway RL (2010) Intraprocedural registration for image-guided kidney surgery. IEEE Trans Mechatron 15(6):847–852. doi:10.1109/TMECH.2010.2066985
16. Benincasa AB, Clements LW, Herrell SD, Galloway RL (2008) Feasibility study for image-guided kidney surgery: assessment of required intraoperative surface for accurate physical to image space registrations. Med Phys 35:4251–4261. doi:10.1118/1.2969064
17. Puerto-Souza GA, Mariottini GL (2013) A fast and accurate feature-matching algorithm for minimally invasive endoscopic images. IEEE-TMI 32(7):1201–1214. doi:10.1109/TMI.2013.223930
18. Glisson CL, Ong R, Simpson AL, Burgner J, Lathrop RA, Webster RJ, Galloway RL (2011) Registration methods for gross motion correction during image-guided kidney surgery. Comput Assist Radiol Surg 6:S159–S163. doi:10.1109/TBME.2012.2215033
19. Cash DM, Sinha TK, Chapman WC, Terawaki H, Dawant BM, Galloway RL, Miga MI (2005) Incorporation of a laser range scanner into image-guided liver surgery: surface acquisition, registration, and tracking. Med Phys 30:1671–1682. doi:10.1118/1.1578911
20. Stoyanov D, Darzi A, Yang GZ (2005) A practical approach towards accurate dense 3D depth recovery for robotic laparoscopic surgery. Comput Aided Surg 10(4):199–208. doi:10.1080/10929080500230379
21. Langø T, Tangen GA, Mårvik R, Ystgaard B, Yavuz Y, Kaspersen JH, Solberg OV, Hernes TAN (2008) Navigation in laparoscopy–prototype research platform for improved image-guided surgery. Minim Invasive Ther Allied Technol 17(1):17–33. doi:10.1080/13645700701797879
22. Mersmann S, Müller M, Seitel A, Arnegger F, Tetzlaff R, Dinkel J, Baumhauer M, Schmied B, Meinzer H-P, Maier-Hein L (2011) Time-of-flight camera technique for augmented reality in computer-assisted interventions. In: Proceeding of SPIE 7964, medical imaging 2011: visualization. Image-guided procedures, and modeling. doi:10.1117/12.878149
23. Maier-Hein L, Groch A, Bartoli A, Bodenstedt S, Guillaume B, Chang P, Clancy N, Elson ND, Haase S (2014) Comparative validation of single-shot optical techniques for laparoscopic 3D surface reconstruction. IEEE-TMI 33(10):1913–1930. doi:10.1109/TMI.2014.2325607
24. Ding S, Miga MI, Noble JH, Cao A, Dumpuri P, Thompson RC, Dawant BM (2009) Semiautomatic registration of pre- and post brain tumor resection laser range data: method and validation. IEEE Trans Biomed Eng 56:770–780. doi:10.1109/TBME.2008.2006758
25. Dumpuri P, Clements LW, Dawant BM, Miga MI (2010) Model-updated image-guided liver surgery: preliminary results using surface characterization. Prog Biophys Mol Biol 103:197–207. doi:10.1016/j.pbiomolbio.2010.09.014
26. Clements LW, Chapman WC, Dawant BM, Galloway RL, Miga MI (2008) Robust surface registration using salient anatomical features for image-guided liver surgery: algorithm and validation. Med Phys 35:2528–2540. doi:10.1118/1.2911920
27. Li P, Wang W, Song Z, An Y, Zhang C (2014) A framework for correcting brain retraction based on an eXtended Finite Element Method using a laser range scanner. Int J CARS 9:669–681. doi:10.1007/s1548-013-0958-8
28. Sirat GY (1992) Conoscopic holography. 1. Basic principles and physical basis. J Opt Soc Am Opt Image Sci Vis 9:70–83. doi:10.1364/JOSAA.9.000070
29. Sirat GY, Psaltis D (1988) Conoscopic holograms. Opt Commun 65:243–249. doi:10.1016/0030-4018(88)90160-5
30. Lathrop RA, Hackworth D, Webster RJ (2010) Minimally invasive holographic surface scanning for soft tissue image registration. IEEE Trans Biomed Eng 57(6):1497–1506. doi:10.1109/TBME.2010.2040736
31. Burgner J, Simpson AL, Fitzpatrick JM, Lathrop RA, Herrell SD, Miga MI, Webster RJ (2012) A study on the theoretical and practical accuracy of conoscopic holography-based surface measurements: toward image registration in minimally invasive surgery. Int J Med Robot 9(2):190–203. doi:10.1002/rcs.1446
32. Simpson AL, Burgner J, Glisson CL, Herrell SD, Ma B, Pheiffer TS, Webster RJ, Miga MI (2013) Comparison study of intraoperative surface acquisition methods for surgical navigation. IEEE Trans Biomed Eng 60:1090–1099
33. Glisson C, Ong R, Clark P, Herrell D, Galloway R (2011) The use of virtual fiducials in image-guided kidney surgery. In: Proceedings of SPIE 7964, medical imaging 2011: visualization. Image-guided procedures, and modeling. doi:10.1117/12.877092
34. Danilchenko A (2011) Fiducial-based registration with anisotropic localization error. Doctoral dissertation, Vanderbilt University
35. Szpala S, Wierzbicki M, Guiraudon G, Peters TM (2005) Real-time fusion of endoscopic views with dynamic 3-D cardiac images: a phantom study. IEEE Trans Med Imaging 24:1207–1215. doi:10.1109/TMI.2005.853639
36. Sielhorst T, Sa W, Khamene A, Sauer F, Navab N (2007) Measurement of absolute latency for video see through augmented reality. In: Proceedings of the 2007 6th IEEE and ACM internationalsymposium on mixed and augmented reality. pp 1–4, 2007. doi:10.1109/ISMAR.2007.4538850
37. https://msdn.microsoft.com/en-us/library/windows/desktop/dd757629(v=vs.85).aspx